Heliyon

ELSEVIER

Received:
19 July 2018
Revised:
11 October 2018
Accepted:
17 December 2018

Cite as: Shaimaa Yousef, Hashem O. Alsaab, Samaresh Sau, Arun K. Iyer. Development of asialoglycoprotein receptor directed nanoparticles for selective delivery of curcumin derivative to hepatocellular carcinoma. Heliyon 4 (2018) e01071. doi: 10.1016/j.heliyon.2018.e01071

Development of asialoglycoprotein receptor directed nanoparticles for selective delivery of curcumin derivative to hepatocellular carcinoma

Shaimaa Yousef[a,1,2], **Hashem O. Alsaab**[a,1,3], **Samaresh Sau**[a], **Arun K. Iyer**[a,b,*]

[a] *Use-inspired Biomaterials & Integrated Nano Delivery (U-BiND) Systems Laboratory Department of Pharmaceutical Sciences, Eugene Applebaum College of Pharmacy and Health Sciences, Wayne State University, Detroit, MI 48201, USA*

[b] *Molecular Imaging Program, Barbara Ann Karmanos Cancer Institute, Wayne State University, School of Medicine, Detroit, MI 48201, USA*

[*] Corresponding author.

E-mail address: arun.iyer@wayne.edu (A.K. Iyer).

[1] Equally contributing authors.

[2] Department of Pharmaceutics and Industrial Pharmacy, Faculty of Pharmacy, Cairo University, Cairo 11562, Egypt.

[3] Department of Pharmaceutics and Pharmaceutical Technology, College of Pharmacy, Taif University, Saudi Arabia.

Abstract

Hepatocellular cellular carcinoma (HCC) is one of the most challenging liver cancer subtypes. Due to lack of cell surface biomarkers and highly metastatic nature, early detection and targeted therapy of HCC is an unmet need. Galactosamine (Gal) is among the few selective ligands used for targeting HCCs due to its high binding affinity to asialoglycoprotein receptors (ASGPRs) overexpressed in HCC. In the present work, we engineered nanoscale G4 polyamidoamine (PAMAM) dendrimers anchored to galactosamine and loaded with the potent anticancer curcumin derivative (CDF) as a platform for targeted drug delivery to HCC. *In vivo* targeting ability and bio-distribution of PAMAM-Gal were assessed via

https://doi.org/10.1016/j.heliyon.2018.e01071

its labeling with the clinically used, highly contrast, near infrared (NIR) dye: S0456, with testing of the obtained conjugate in aggressive HCC xenograft model. Our results highlighted the targeted dendrimer PAMAM-Gal ability to achieve selective high cellular uptake via ASGPR mediated endocytosis and significantly enhance the delivery of CDF into the studied HCC cell lines. Cytotoxicity MTT assays in HCC cell lines, interestingly highlighted, the comparative high potency of CDF, where CDF was more potent as a chemotherapeutic anticancer small molecule than the currently in use Doxorubicin, Sorafenib and Cisplatin chemotherapeutic agents. In conclusion the proof-of-concept study using nanoscale PAMAM-Gal dendrimer has demonstrated its competency as an efficient delivery system for selective delivery of potent CDF for HCC anticancer therapy as well as HCC diagnosis via NIR imaging.

Keywords: Pharmaceutical chemistry, Materials science, Pharmaceutical science

1. Introduction

Liver cancer is a neoplasm that affects the hepatic tissues. According to WHO, liver cancer was documented as the second most common lethal cancer worldwide in 2012 [1]. In contrary to the declining trend of most cancer types, liver cancer presented increased incidence and mortality rates, indicating its poor prognosis [2, 3]. American cancer society, estimated 42,220 new cases of liver cancer to occur in the US during 2018 [4]. Histological analysis suggested that hepatocellular carcinoma (HCC) contributes to 75−90% of liver cancer [5]. It originates mostly in inflamed and cirrhotic liver, with the most commonly recognized causes being the Hepatitis B (HBV) and Hepatitis C (HCV) infections [6, 7]. Other risk factors as aflatoxin B1 ingestion, non-alcoholic fatty liver, alcohol consumption, iron overload in hemochromatosis [8] and type 2 diabetes [9] also have a correlation with HCC.

In terms of HCC treatment strategies, they are multiple and various depending on the tumor size, the liver functionality, as well as the number of lesions and stage. Surgical liver resection is mostly performed in case of single non-cirrhotic tumor lesion, other than in cases of cirrhosis and multiple invasive tumor foci. Cases of cirrhotic and multiple lesions are more susceptible to post resection tumor relapse [10, 11]. Patients who are not candidates for resection, are managed by different invasive but non-surgical therapeutic approaches including local radiotherapy (LR), percutaneous ethanol injection (PEI) [12], trans arterial chemoembolization (TACE) [13], and radiofrequency ablation (RFA) [14]. Liver transplantation is another HCC therapeutic module, however it is a big and expensive procedure that takes long time to find the right matched liver donor, and needs post-operative immunosuppressive treatment to avoid rejection [10, 15].

https://doi.org/10.1016/j.heliyon.2018.e01071

Unfortunately, more than 80% of HCC patients are lately diagnosed at an advanced stage where the above curative therapeutic modalities would not be effective [16, 17]. Systemic chemotherapeutic drugs such as cytotoxic drugs or antiangiogenic agents are the main treatment of choice for those advanced stage HCC patients. In addition, systemic chemotherapies are also important with other therapeutic strategies since they are administered as adjuvant therapies with other treatment options. Systemic cytotoxic agents such as doxorubicin, 5-fluorouracil, epirubicin, and cisplatin were used for advanced HCC either solo or in combination; however, very low efficacy with no more than 20% response rate was accomplished [16, 17]. Antiangiogenic agents such as sorafenib, erlotinib, and Bevacizumab are also reported to play a role in HCC management through the suppression of the tumor's ability to generate new blood vessels [18, 19]. Currently, checkpoint inhibitors against programmed death-1 (PD-1), programmed death ligand-1 (PD-L1), CTL-4 has demonstrated significantly better therapeutic outcomes in multiple cancers, including HCC [20]. The blocking of immune-check point molecules resurrect the T-cell mediated cancer cell killing that revalorized the current cancer therapy [21, 22, 23] and this discovery was recognized by 2018 Nobel prize in medicine. .

In terms of cancer chemotherapy, the low responsive rate and the poor therapeutic outcomes of systemic cytotoxic agents are related in a way or more to several physicochemical properties of drugs such as their molecular weight, stability, and hydrophobicity, in addition to related pathophysiological factors such as drugs inefficient accumulation in tumor lesions, as well as various cancer cells chemo-resistance mechanisms [19, 24, 25, 26]. Consequently, in order to increase and improve therapeutic responses in HCC cases, there is urgent need to try to overcome the mentioned factors that participate in diminishing the cytotoxic drugs' efficacy.

In this regard, improving the chemotherapeutic drugs accumulation in cancer cells through active targeting of cancer tissues, as well as the use of more potent drugs are good means that are supposed to help increase therapeutic response rates. 3,4-difluoro-benzylidene-curcumin (CDF) is curcumin fluoro synthetic analogue [27, 28, 29, 30]. CDF is a hydrophobic potent anticancer agent that showed antitumor activity in different cancer types [31, 32, 33]. The CDF anticancer activity was attributed to several mechanisms. CDF is an efficient proteasome inhibitor and apoptosis inducer in pancreatic cancer cell lines [27, 34]. Matrix metalloproteinase protein MMP-2 expression and activity are highly inhibited by CDF leading to suppression of tumor invasion and metastasis [35]. CDF showed potent anticancer activity in pancreatic cancer stem cells with inhibition of pancreatic tumor sphere formation. The mechanism of anticancer activity of CDF is associated with inhibition of NF-kB binding to DNA, inhiation of COX-2 expression, downregulation of the miR-21 oncogene expression, and up-modulation of the tumor suppressor miR-200 gene both in vitro [36] and in vivo [29, 37].

https://doi.org/10.1016/j.heliyon.2018.e01071

Entrapment of CDF in one of the nano-carriers can overcome its hydrophobicity, improve its water solubility, its stability and its systemic delivery in a way that helps in CDF passive accumulation in tumor tissues. Targeting ligand galactosamine is among the selective ligands used for actively targeting HCCs due to its high binding affinity to asialoglycoprotein receptors [38, 39, 40]. Asialoglycoprotein lectin receptors (ASGPRs), also known as (Ashwell receptor) are receptors that were found to be overexpressed in several human tumorous hepatocytes [41] and HCC cell lines including Hep G2 and Huh7.5 cells [42, 43]. ASGPRs internalize molecules exposing the carbohydrate residue galactosamine through clathrin type receptor mediated endocytosis [40, 44]. Galactosamine achievement of ASGPR mediated efficient liver cancer targeting was documented in phase I clinical trial of poly[N-(2-hydroxypropyl)methacrylamide] copolymer carrying doxorubicin and galactosamine, as reported by Julyan et al. [45]. In the present work, we engineered G4 PAMAM dendrimers which can be multifunctional in use and can be utilized as modular platform for delivering anticancer drugs and/or imaging agents simultaneously or individually, in a targeted manner to liver cancer type [46, 47]. The multifunctional terminology is used to indicate that the GAL-decorated G4 PAMAM can function as a both therapeutic and imaging agent delivery system of asialoglycoprotein receptor overexpressing tumors, such as liver and colon cancer [48]. Our delivery system is composed of galactosamine anchored G4 PAMAM dendrimers loaded with the new potent anticancer drug CDF.

2. Materials and methods

2.1. Chemical reagents and cell cultures

Curcumin analogue derivative CDF was synthesized as described earlier [30, 33, 49, 50]. Fourth generation (4.0G) PAMAM dendrimer, N-(3-(dimethylamino) propyl)-N-ethylcarbodiimide hydrochloride (EDC), and 3-[4,5 dimethylthiazol-2-yl]-2,5diphenyltetrazolium bromide (MTT) were obtained from Sigma-Aldrich (St. Louis, MO). GA was purchased from Fisher Scientific. All other chemicals were of reagent grade and used without any further modification. Human liver cancer cells (HepG2 cells) was used for our study due to documented evidence of over-expression of ASGPR receptors. HepG2 cells were cultured in Dulbecco's Modified Eagle's Medium (DMEM; Fisher Scientific, Waltham MA). All media were supplemented with fetal bovine serum (10% v/v), glucose (4.5 g/L), l-glutamine (292 mg/L), and streptomycin sulfate (10 mg/L). All cell lines were incubated in a 5% CO_2 air humidified atmosphere at 37 °C.

2.2. Synthesis experimental and characterizations

Galactosamine targeted G4 PAMAM dendrimers (PAMAM-Gal) in which galactosamine moieties were attached to PAMAM dendrimers through succinic acid linker,

https://doi.org/10.1016/j.heliyon.2018.e01071

were synthesized in two steps. First, the G4 PAMAM dendrimers (250 mg, 0.0176 mmol) was dissolved in 10mL dimethyl sulfoxide (DMSO). Then, 20 fold excess succinic anhydride (2253.5 mg, 22.53 mmol) was added to the solution and the reaction mixture was stirred at 55 °C for 24 hours [50]. The product of PAMAM dendrimers attached to succinic moieties (PAMAM-Succ) was dialyzed using a dialysis bag (MWCO 12-14KDa, Spectra/Por, Spectrum Labs, San Diego, CA, USA) against deionized water for 2 days with frequent changes to the dialysis water to remove solvents, and any small molecular weight unreacted succinic acid reagent. The dried final product PAMAM-Succ was obtained by lyophilization.

In the next step, PAMAM-Succ product obtained in the first step was reacted with galactosamine. HCl as follows [51]: PAMAM-Succ (120 mg) was dissolved in 12 mL (Na_2HPO_4/NaH_2PO_4) phosphate buffer pH 7.8, then 1-ethyl-3-(3-dimethylamino) propyl carbodiimide, hydrochloride (EDC) (143 mg, 0.75 mmol) and sulfo *N*-hydroxysuccinimide (sulfo NHS) (162 mg, 0.75 mmol) were added to the solution, and the mixture was kept under stirring on ice for 1 hour. Galactosamine. HCl (104 mg, 0.484 mmol) was dissolved in 5 ml (Na_2HPO_4/NaH_2PO_4) phosphate buffer with the addition of trimethylamine drops to the solution till pH of 7.4. The solution of the galactosamine in its basic form was added to the above activated PAMAM-Succ solution and was stirred at room temperature for 24 hours. The product was dialyzed using a dialysis bag (MWCO 12-14KDa, Spectra/Por, Spectrum Labs, San Diego, CA, USA) against deionized water for 3 days with frequent changes to the dialysis water to remove salts and any small molecular weight unreacted reagents. The dried final product, PAMAM-Gal was obtained by lyophilization. The successful synthesis of PAMAM-Gal product was confirmed by Fourier transform infrared spectroscopy (JASCO, FT/IR - 4200 Fourier Transform Infrared Spectrometer, Japan) and Proton nuclear magnetic resonance (^1H NMR) spectroscopy (600 MHz, Agilent-NMR-inova600, Santa Clara, CA, USA).

2.3. Drug encapsulation and loading

CDF was encapsulated in plain PAMAM and PAMAM-Gal separately using equilibrium dialysis method as described earlier [49, 50]. In brief, CDF/G4-PAMAM-Gal and CDF/G4-PAMAMF nanoformulations at the molar ratio of 50:1 were dissolved in DMSO/phosphate buffered saline (PBS) pH 7.4 (ratio 4:6). The solution was stirred in the dark after mixing them at a slow speed (50 rpm) for 48 h. at RT. Then, the incubated solution was then dialyzed against DIW under strict sink condition using dialysis bag (MWCO 3.5 kDa, Sigma), followed by filtration to remove un-encapsulated CDF, and was lyophilized, stored and utilized for all characterization, and later the product was evaluated for solubility under dark conditions. To quantify the amount of CDF loaded in both CDF/G4-PAMAM-Gal and CDF/G4-PAMAM, the lyophilized powder were dissolved in DIW and measured the

https://doi.org/10.1016/j.heliyon.2018.e01071

absorbance at 447 nm using either UV−vis spectrometry (Jasco 530 UV−vis spectrometer, Tokyo, Japan) or HPLC system as the method was previously described [49, 50]. The encapsulation efficiency (EE %) and drug loading content (DLC) of CDF/G4-PAMAM and CDF/G4-PAMAM were obtained by high-performance liquid chromatography (HPLC) analysis. The lyophilized product was dissolved in deionized water. Then the sample was quantitatively analyzed by HPLC. The mobile phase consisted of 70% methanol, 29.55% water and 0.45% formic acid (v/v/v) with 1 ml/min flow rate. The injection volume was 10μL and it was performed in triplicate. The UV detection wavelength in HPLC were set at 447 nm. The EE% and DLC were calculated by the following equations:

$$EE\ (\%) = \frac{Amount\ of\ CDF\ in\ dendrimer}{Amount\ of\ CDF\ used} \times 100$$

$$DLC(\%) = \frac{Amount\ of\ CDF\ in\ dendrimer}{Total\ amount\ of\ dendrimer} \times 100$$

2.4. Size and zeta potential measurements (LS)

Hydrodynamic size and zeta potential measurements of plain G4 PAMAM dendrimers, and G4 PAMAM dendrimers attached to galactosamine targeting moieties (PAMAM-Gal) were performed in triplicates using Light Scattering (LS) analysis. All samples were tested in a Zetasizer Nano ZS (Malvern Instruments, Westborough, MA, USA) at 25 °C. Plain G4 PAMAM and PAMAM-Gal samples were prepared in DIW at concentration of (2 mg/ml) and (1 mg/ml) for size and zeta potential determination, respectively. Plain G4 PAMAM and PAMAM-Gal sizes were measured at a volume of 350 μl using disposable cuvettes, while their surface charge or zeta potentials (ζ) were tested at a volume of 750 μl using transparent zeta cuvettes and using the same instrument. The scattered light detection was at 173° backscatter angle, distilled water viscosity and refractive index of (0.8872 cP) and (1.33), respectively, were set as measuring parameters. Triplicate samples where tested, and three measurements were performed for each sample with at least 12 runs per each measurement. Results of size and zeta measurements were presented in Table 1 as Z-average hydrodynamic size in nanometers (±SD, n = 3) and mean in millivolts, mV (±SD, n = 3), respectively.

2.5. Morphology and size measurements (TEM)

The size and morphology of plain G4 PAMAM and PAMAM-Gal dendrimers in the dry state were obtained by transmission electron microscopy (TEM). TEM samples were prepared by adding a drop of plain G4 PAMAM or PAMAM-Gal dendrimers solution (2 mg/ml) on a copper-coated grid (200 mesh) for 3 minutes followed by blotting the grid and staining using 3% uranyl acetate staining solution for another 3 minutes. Finally, the grid was dried completely in air before imaging. Nanopure

https://doi.org/10.1016/j.heliyon.2018.e01071

Table 1. Characterization of G4 PAMAM dendrimer nanoformulations.

Sample	Hydrodynamic size (nm)	PDI	Zeta potential (mV)	Conductivity (mS/cm)	EE (%) with addition of CDF
PAMAM-Gal (Targeted)	48.7 ± 7.03 nm	0.69 ± 0.02	−8.3 ± 1.24	0.0256	75.5 ± 12
G4-PAMAM (non-targeted)	9.97 ± 3.76 nm	0.23 ± 0.07	13 ± 3.23	0.0358	85 ± 9.8

Abbreviations: G4-PAMAM, Polyamine dendrimer; GAL, Galactosamine; PDI, polydispersity index; EE, encapsulation efficiency.

deionized water was used as the dispersion medium for preparing samples. Various images were obtained for each sample with a transmission electron microscope (JEOL 2010 TEM, LaB6 Filament Gun, Tokyo, Japan) at an accelerating voltage of 200 kV and 100,000× magnification.

2.6. Cytotoxicity assays (MTT)

The *in vitro* cytotoxicity of free drugs Curcumin, Cisplatin, Sorafenib, doxorubicin, and CDF (and its dendrimer formulations CDF/G4-PAMAM-Gal and CDF/G4-PAMAM), as well as the cytotoxicity of the plain carriers (G4 PAMAM and PAMAM-Gal) were studied and compared using MTT assay on HepG2 human HCC cells. The Hep G2 cells were seeded in 96 well plates at cell density of 5000 cells/well in 100 μL of DMEM growth medium containing 10% FBS and incubated for 24 hours at 37 °C in humidified air containing 5% CO_2. Stock solutions of different drugs were prepared in DMEM growth medium after dissolution in sterile dimethyl sulfoxide (DMSO). Predetermined concentrations were obtained by serial dilution of the respective stock solutions with cell culture medium supplemented with FBS. Subsequently, 100 μL of each serial dilution was added on the preexisting 100 μL media in each well to achieve final drug concentrations ranging from 0.5 to 50 μM. The cells were incubated either for 24 or 48 hours. MTT solution in phosphate buffered saline (PBS; 5 mg/mL) was then added to cells (20 μL/well), and the plates were incubated for additional 3 hours at 37 °C and 5% CO_2. Then, all the media were removed and 100 μL of dimethyl sulfoxide (DMSO) was added in each well and the plates were subjected to orbital shaking in the dark for 15 minutes. The DMSO solvent dissolved the purple colored formazan crystals formed in the mitochondria of live cells.

The absorbance was recorded at 590 nm on a synergy 2 microplate reader (BioTek Instrument, Winooski, VT, USA). Results were presented as mean (±SD, n = 6) of relative cell viability (%). Percentage relative cell viability = (treated cells absorbance − blank absorbance)/(untreated cells absorbance − blank absorbance) ч 100. Treated and untreated cells are cells cultured in presence or absence of drugs, respectively. Blank values (controls) were referred to the absorbance measured in wells that did not contain cells.

https://doi.org/10.1016/j.heliyon.2018.e01071

2.7. Fluorescence microscopic study

All formulations were firstly labeled with Rhodamine B (red fluorescence dye) at a molar concentration of dendrimer formulation to Rhodamine B of 5:1 and incubated in DIW for 8 h at room temperature with intermittent mixing. HepG2 human HCC cells (5×10^4) were seeded in six-well plate and incubated at 37 °C under 5% CO_2 for 24 h. The media was replaced with 2 ml of serum-free, antibiotic-free medium and treated with various concentrations of labeled formulations and incubated for 2 h. The formulations containing medium was removed, and resulting cells were washed thrice with PBS and fixed with 2% formaldehyde in the PBS at room temperature for 15 min. Nuclei were stained with a blue fluorescence dye (Hoechst 3342, Thermo Fisher Scientific, Waltham, MA) at RT for 5−10 min and samples were quantitatively analyzed using fluorescence microscopy [52, 53, 54, 55].

2.8. Animal husbandry and In vivo NIR imaging and biodistribution study

6−8 weeks old nu/nu female mice were purchased from Jackson Laboratories, housed in a sterile environment on a standard 12 h light/dark cycle and kept on normal rodent diet and water. All animal procedures were approved by the Wayne State Animal Care and IACUC committee in accordance with National Institutes of Health guidelines. Mice were injected subcutaneously with HepG2 human HCC cells in PBS medium (5.0×10^6 cells per mouse). Tumor growth was measured in two perpendicular directions every 2 days with a caliper. Tumor volumes were calculated using formula $0.5 \times a \times b^2$, where a is the measurement of the longest axis and b is the measurement of the axis perpendicular to L. Tumor bearing mice were treated via tail vein injection with PAMAM-GAL-S0456 at a S0456 dye concentration of 10 nmole/mice in the dye conjugate. Mice were imaged 14 h post injection using a Carestream In Vivo MS FX Extreme, Light Source: 400 W Xenon, Monochrome interlined, fixed lens (10x), cooled (−60 °C), CCD camera, excitation 750 nm, emission 830 nm wavelength for fluorescence, and X-ray images were captured. Both fluorescence and X-ray images of mouse was merged to demonstrate the localization of nanoparticles. Importantly, to more understand the target ability in tumor and healthy tissues, bio-distribution at 14 h post-injection for major organs/tissues were examined for NIR fluorescence.

3. Results

3.1. Synthesis and confirmation of PAMAM- GAL conjugate

PAMAM-Gal dendrimers were synthesized in two steps through amide bonds formation (Figs. 1 and 2). In the first step, opening of the anhydride ring in succinic anhydride acids (**1**) by terminal primary amine groups on the surface of G4 PAMAM

https://doi.org/10.1016/j.heliyon.2018.e01071

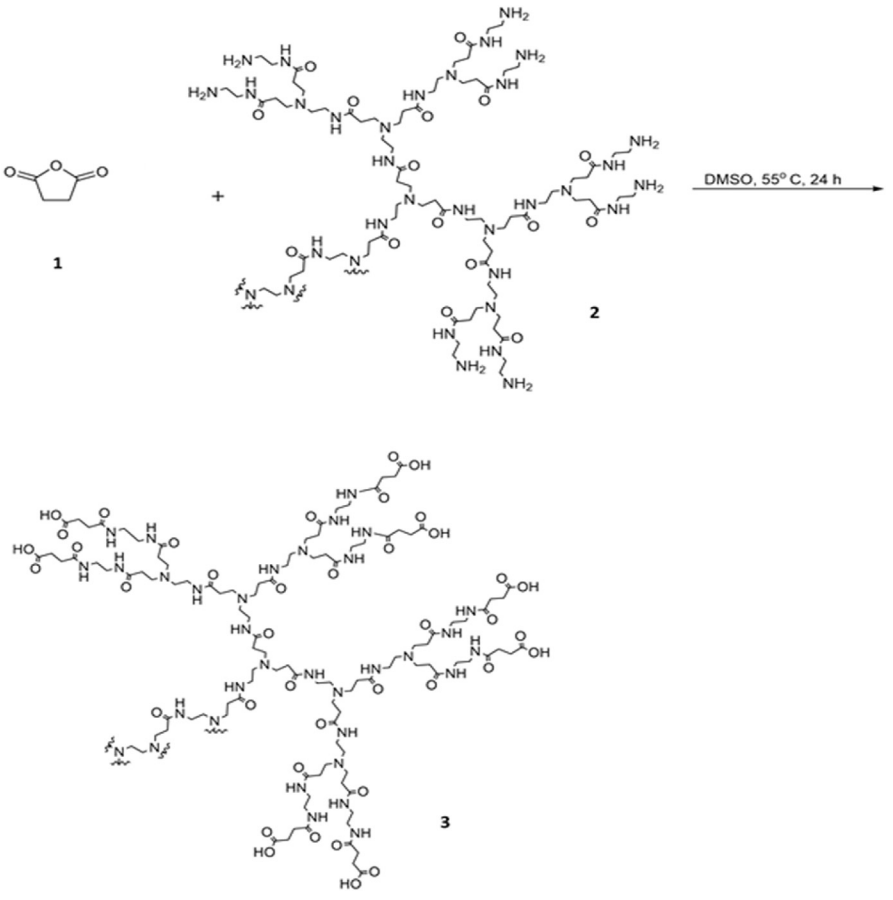

Fig. 1. PAMAM-Succ Synthesis. Opening of the anhydride ring in succinic anhydride acids (**1**) by terminal primary amine groups on the surface of G4 PAMAM dendrimers (**2**) to form amide bond links and obtain the PAMAM-Succ product (**3**). The reaction mixture was stirred in DMSO at 55 °C for 24 hours.

dendrimers (**2**) to form amide bond links and obtain the PAMAM-Succ product (**3**) was undertaken. In the second step, coupling of sulfo *N*-hydroxysuccinimide esters of PAMAM-Succ with amine group in galactosamine. HCl (**4**) in its basic form was performed. The coupling reaction resulted in amide bond formation and PAMAM-Gal dendrimers product (**5**) were obtained.

The structural characterization of PAMAM-GAL conjugate and the synthesized products were confirmed by FTIR spectroscopy (Fig. 3) and ^{1}H NMR (Fig. 4).

FT-IR (ν, cm^{-1}): spectrum showed masking of PAMAM-Succ (2500−3500 carboxylic acid broad −OH stretch), 3322 (amide −NH stretch, and alcohol −OH stretch), 2972−2885 (aliphatic −CH stretch), 1641 (secondary amide −C=O stretch), 1541 (amide -NH deformation), 1086 (alcohol − C-OH stretch).

^{1}H NMR (d_2-D_2O): spectrum demonstrated peaks of δ (ppm) = 2.2 (-$NCH_2C\mathbf{H}_2CONH$-), 2.3−2.6 (overlapping peaks of: -$COC\mathbf{H}_2CH_2CO$-Gal, -$NC\mathbf{H}_2CH_2NHCO$-, and -$COCH_2C\mathbf{H}_2CO$-Gal), 2.7−3.4 (overlapping peaks of:

https://doi.org/10.1016/j.heliyon.2018.e01071

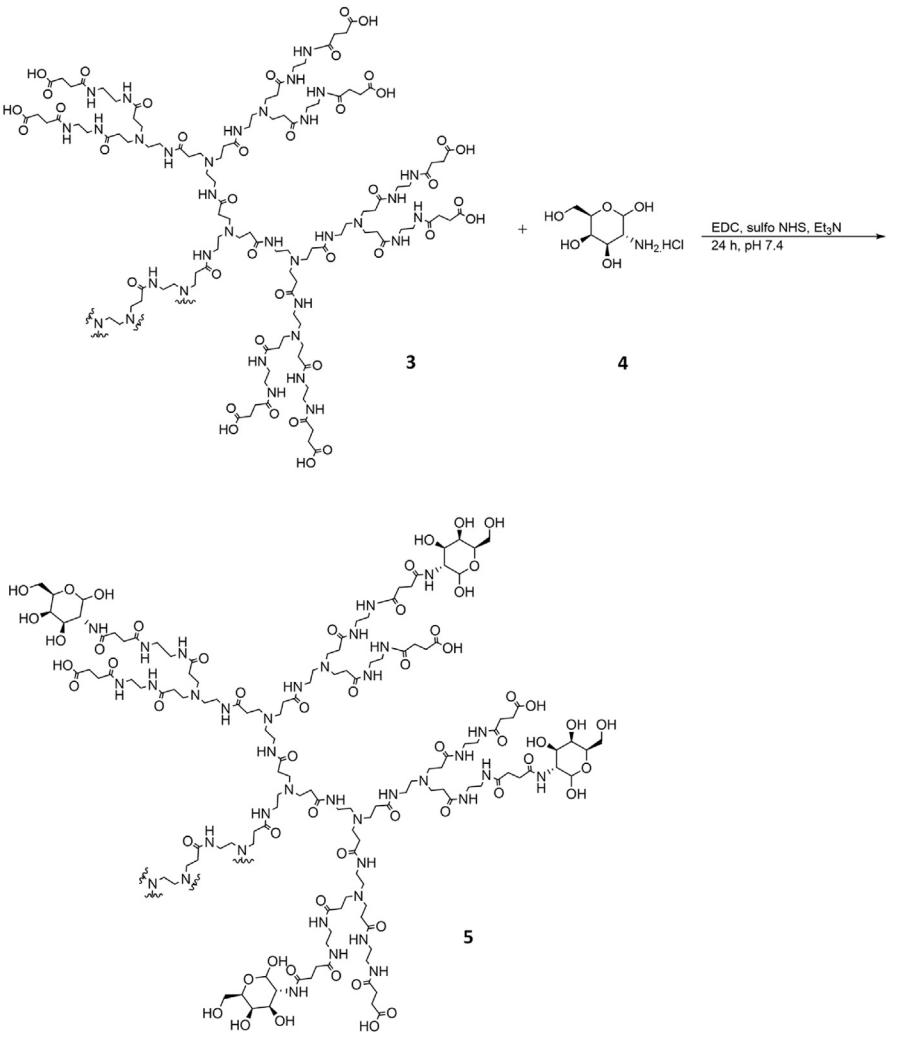

Fig. 2. PAMAM-Gal Synthesis. Coupling of sulfo *N*-hydroxysuccinimide esters of PAMAM-Succ with amine group in galactosamine. HCl (**4**) in its basic form. The reaction was performed at pH 7.4 for 24 hours. Amide bonds were formed and PAMAM-Gal product (**5**) was obtained.

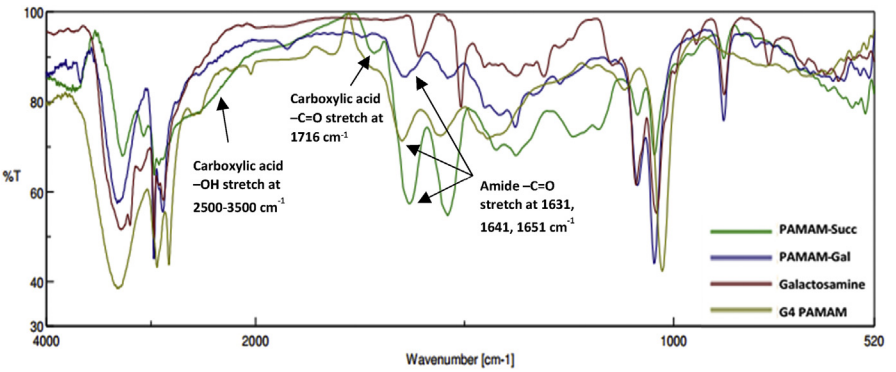

Fig. 3. Overlay of the FT/IR spectra of PAMAM-Succ (green), PAMAM-Gal (blue), Galactosamine (red), and G4 PAMAM (greenish yellow). Characteristic peaks are marked as shown on the spectra.

https://doi.org/10.1016/j.heliyon.2018.e01071

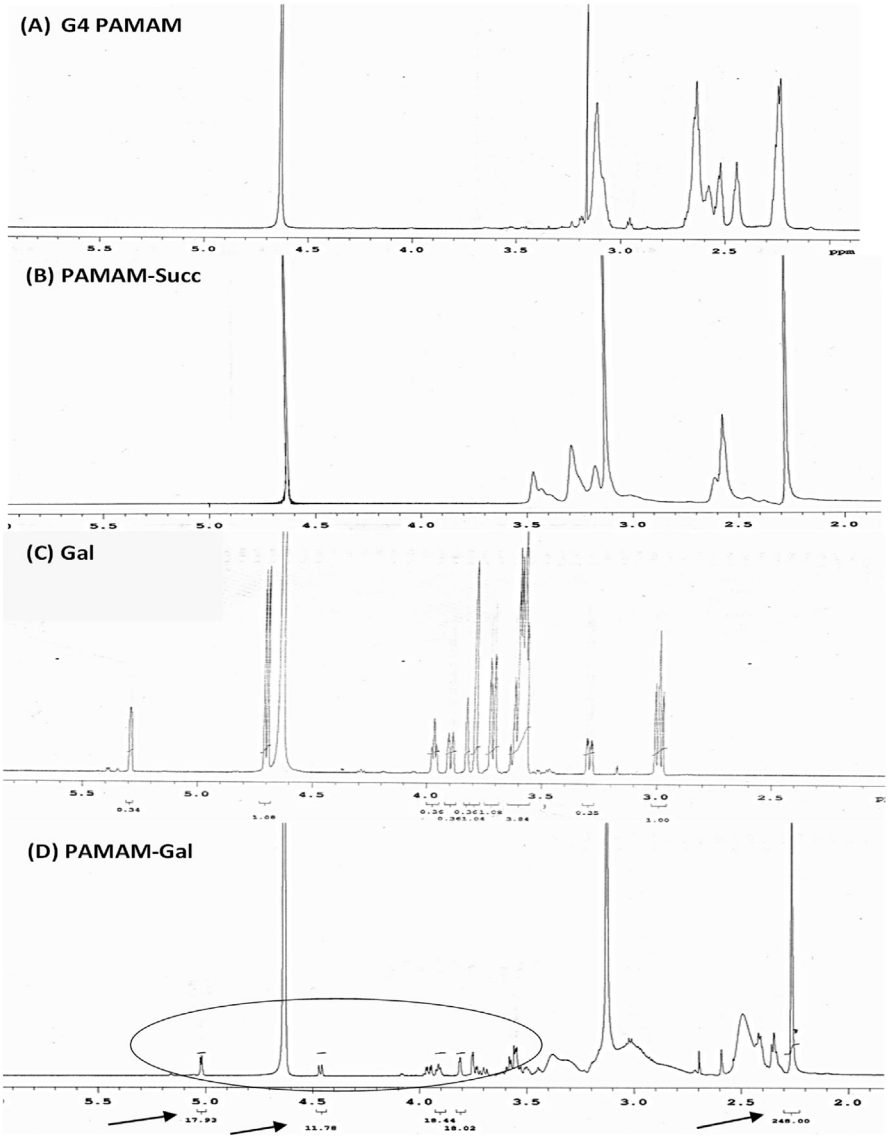

Fig. 4. Proton nuclear magnetic resonance (^{1}H NMR) spectra of: (A) G4 PAMAM (B) PAMAM-Succ (C) GAL (D) PAMAM-GAL. The ^{1}H NMR spectrum of PAMAM-GAL showed the characteristic integrated peaks as described. Characteristic peaks of PAMAM dendrimers and their products are included.

-NC**H**$_2$CH$_2$CONH -, -NCH$_2$C**H**$_2$NHCO-, -NHC**H**$_2$C**H**$_2$NH-, and −C**H**NHCO- protons in galactosamine alpha and beta anomers), 3.5−3.6 (-C**H**$_2$OH, -C**H**CH$_2$- protons in galactosamine alpha and beta anomers), 3.7 (-NHCHC**H**CH- protons in galactosamine alpha anomers), 3.75 (-C**H**CHCH$_2$OH - protons in galactosamine alpha anomers), 3.8 (-C**H**CHCH$_2$OH - protons in galactosamine beta anomers), 3.9 (-C**H**CH$_2$OH protons in galactosamine beta anomers), 3.95 (-NHCHC**H**CH- protons in galactosamine beta anomers), 4.45 (-OC**H**OH alpha anomeric protons in galactosamine), 5 (-OC**H**OH beta anomeric protons in galactosamine). As presented in Fig. 4, structural characterization confirmed by ^{1}H NMR and the peaks

https://doi.org/10.1016/j.heliyon.2018.e01071

integration in the PAMAM-Gal spectrum showed that around 30 galactosamine molecules get attached on each PAMAM dendrimer. The 30 galactosamine molecules were 12 alpha and 18 beta anomers as demonstrated in the ^{1}H NMR spectrum. As a result, the PAMAM-Gal product molecular weight was calculated to be 25455.97 gm compared to 14214.17 gm for plain G4 PAMAM.

3.2. Characterization of PAMAM-GAL dendrimers

3.2.1. CDF drug loading and encapsulation

Dendrimer based formulations were found to be completely water soluble compared to free CDF drug. CDF was encapsulated in PAMAM and PAMAM-GAL conjugate using equilibrium dialysis method. The CDF loading in CDF/G4-PAMAM-GAL was higher than in CDF/G4-PAMAM. It was found to be 17.7% ± 5.43% w/w and 13.5% ± 3.70% w/w, respectively. Also, the CDF/G4-PAMAM-GAL EE% was found to be 85% ± 9.8% and for CDF/G4-PAMAM was found to be 75.5% ± 12% and that results revealed the addition of GAL to the dendrimer formulation might be the reason of the increase in the EE%.

3.2.2. Size, zeta potential, and morphology by transmission electron microscopic (TEM) analysis

Light scattering techniques as well as Transmission Electron Microscopy were used to evaluate size, zeta potential, and morphology of the nanoformulations. As shown in Fig. 5, results were presented as mean (±standard deviation) from three independent experiments. PAMAM-Gal dendrimers exhibited larger hydrodynamic diameter of 48.7 ± 7.03 nm than plain G4 PAMAM dendrimers whose size was around 9.97 ± 3.76 nm. Plain G4 PAMAM dendrimers had positive zeta potential of around 13 mV ± 3.23 because of the terminal protonated amine groups, while the galactosamine decorated PAMAM (PAMAM-Gal) showed a negative zeta potential of -8.3 ± 1.24 mV due to the presence of anionic uncoupled succinic carboxylic groups on the PAMAM surface. Polydispersity index (PDI) as an indication of size distribution of plain G4 PAMAM and PAMAM-Gal dendrimers was found to be 0.23 ± 0.07 and 0.69 ± 0.02, respectively.

To further determine the size of the G4 PAMAM and PAMAM-GAL dendrimers in the dry state, electron microscopic analysis was performed. TEM images illustrated both the size and morphology of plain G4 PAMAM and PAMAM-Gal dendrimers (Fig. 5). TEM images of the G4 PAMAM and PAMAM-Gal particles indicated their nano-metric size range (Fig. 5C and D). Spherical structure of the dendrimers was obvious in the images as plain G4 PAMAM showed a size of around ~4 nm, while PAMAM-Gal dendrimers showed a size of ~21 nm. The TEM sizes, in the dry

https://doi.org/10.1016/j.heliyon.2018.e01071

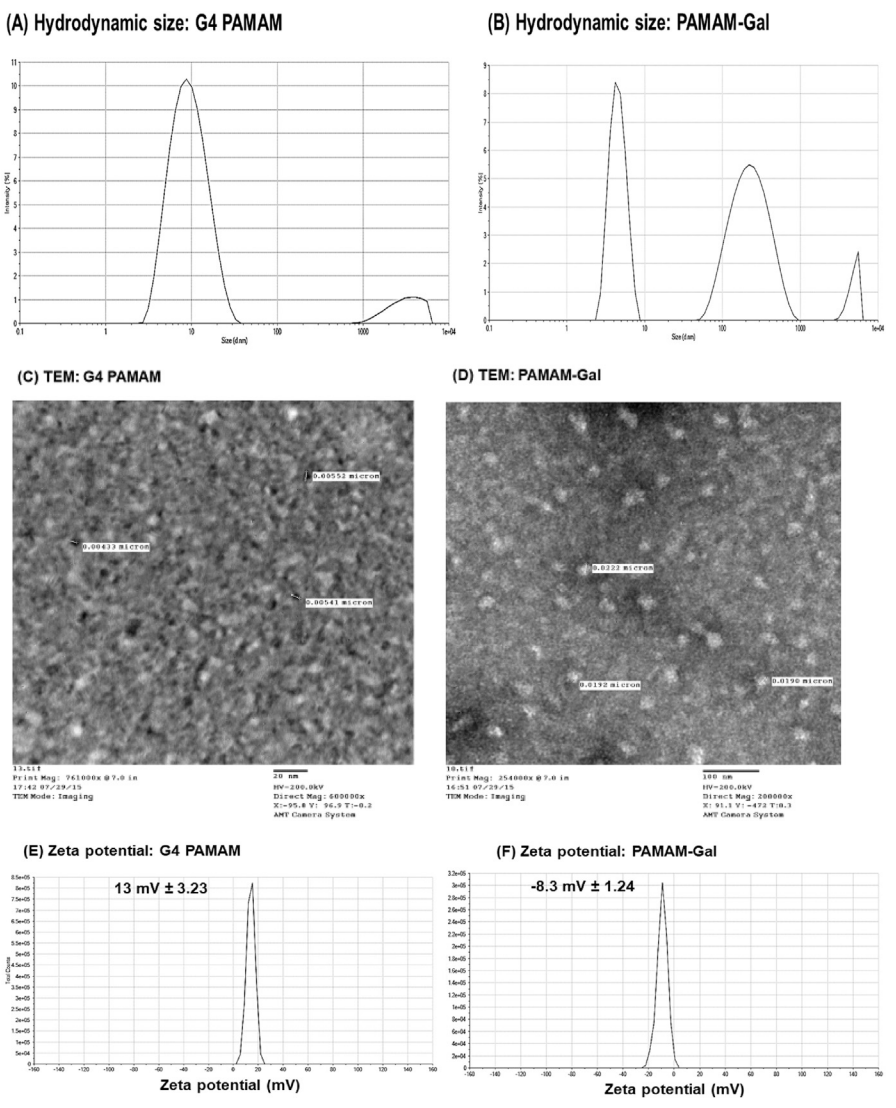

Fig. 5. (A & B) Hydrodynamic size of plain and targeted dendrimers in nanometers by (DLS); (C & D) Morphology and size measurements of G4 PAMAM and PAMAM-GAL dendrimers characterized by TEM are shown, with scale bar = 20 nm, and 100 nm respectively; and (E & F) Zeta potential measurements of both dendrimers in millivolts.

state, although were relatively smaller but they were in accordance with the ones obtained from DLS measurements, which is the hydrodynamic size.

3.3. In vitro cytotoxicity assay

CDF, doxorubicin, sorafenib and cisplatin plain drugs comparative cytotoxicity's were studied on HCC cell line Hep G2 by MTT cytotoxicity assay. The results demonstrated that the drugs cytotoxicity was in the following order: CDF > sorafenib > doxorubicin > cisplatin (Fig. 6) for 48 hrs as shown in Fig. 6. CDF was found

https://doi.org/10.1016/j.heliyon.2018.e01071

to be more potent than sorafenib, doxorubicin, and cisplatin on Hep G2 cell line where they showed an IC_{50} of around 4 μM, 8 μM, 12 μM, and 22 μM, respectively.

In addition, the ability of CDF/G4-PAMAM and CDF/PAMAM-GAL to exert their anticancer response was tested on ASGPRs receptor overexpressing cells by *in vitro* MTT cytotoxicity assay. The results showed a dose-dependent cell killing for both CDF/G4-PAMAM and CDF/G4-PAMAM-GAL nanoformulations. The result of the experiment revealed an IC_{50} of 4 ± 0.2 μM, 1 ± 0.3 μM, and 2 ± 0.01 μM for CDF, CDF/PAMAM-GAL and CDF/G4 PAMAM, respectively in Hep G2 cells. Interestingly, G4 PAMAM and PAMAM-GAL dendrimers showed nontoxic behavior at the concentrations used indicates that they could be promising carriers for anticancer drug delivery.

3.4. Fluorescence microscopic study

Fluorescence microscopic study was performed to compare the level of cellular uptake of the non-targeted formulation PAMAM and the targeted formulation PAMAM-GAL. As shown in Fig. 7, the fluorescence intensity of Rhodamine B – labeled dendrimer formulations was obvious indicating their uptake. Comparatively, higher uptake was observed in case of targeted formulation PAMAM-GAL-Rhodamine B, and it could be attributed to better uptake of the formulation via ASGPRs receptors mediated endocytosis (Fig. 7). Our results are in accordance

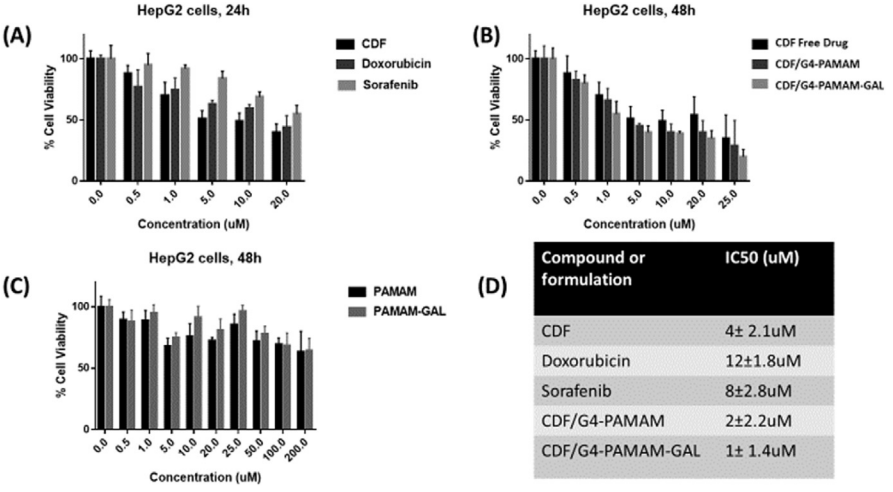

Fig. 6. (A) Cytotoxicity assay of Plain Drugs after 48h (B) Cytotoxicity Assay of free CDF, G4-PAMAM-CDF, and G4-PAMAM-GAL-CDF after 48h (C) Cytotoxicity Assay of plain PAMAM, PAMAM-GAL showed that they were safe at higher concentrations and conjugation with GAL reduced the cytotoxicity. Data represented as mean (±SD, n = 6). (D) Summary of IC50s is represented using GraphPad Prism software® as shown. The histogram columns represent means of three independent experiments with 6 replicates for each treatment; bars, S.E. Figures (A–C), $p \leq 0.05$* and ** statistically significant inhibition (*$p \leq 0.05$) relative to DMSO-treated respective controls or (**$p \leq 0.05$) relative to CDF drug treated cells.

https://doi.org/10.1016/j.heliyon.2018.e01071

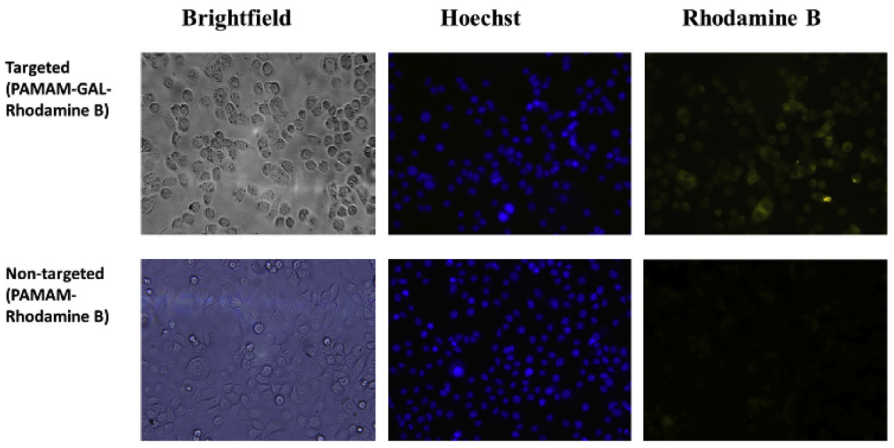

Fig. 7. Fluorescence microscopic study. Cancer cell selective uptake of Rhodamine B labeled targeted dendrimers than the non-targeted dendrimers in HepG2 cells after 2 h treatment. Blue and red fluorescence indicate cell nuclei and Rhodamine B, respectively.

with previous studies which showed higher fluorescence intensity with targeted formulation and that could be a useful feature in inducing cancer cell selective cytotoxicity [55, 56].

3.5. Animal imaging and bio-distribution study with HCC mice model

Since HCC frequently detected at late stage and it has high metastatic tendency, thus the early detection of tumor mass is one of unmet and urgent needs for surgical resection. Also, near infrared (NIR) imaging is a cost effective, less toxic, and advanced diagnostic tool for tumor detection. To determine the *in vivo* HCC targeting efficacy of PAMAM-GAL, we conjugated the clinically used, high contrast, structurally symmetrical near infrared dye (S0456) to arrive at PAMAM-GAL- S0456 as targeted formulation [57, 58]. Hep G2 tumor bearing mice were injected with PAMAM-GAL-S0456 and whole-body imaging was performed as mentioned in experimental section. As shown in Fig. 8 A, GAL-targeted conjugated dendrimers were predominantly accumulated in ASGPRs overexpressed HepG2 tumor. Biodistribution results and the Fluorescence intensity of tumor (Fig. 8B) suggested that PAMAM-GAL-S0456 was accumulated in liver cancer. Clinically translatable imaging agent required faster clearance from the body and excretion of imaging agent through kidney route reduces the toxicity as compared to liver. NIR imaging of PAMAM-GAL-S0456 indicates as (Fig. 8C and D) showed that low liver uptake compared to kidney. Control nanoparticle-dye treated mice revealed low tumor tumor uptake (Fig. 8E). This favors the rational for developing HCC selective tumor imaging agent and for imagining guided surgery [53]. Overall, ASGPRs receptor-targeting dendrimer had potential to distinguish the tumor lesion and had kidney mediated excretion that can be further developed orthotropic HCC tumor model.

https://doi.org/10.1016/j.heliyon.2018.e01071

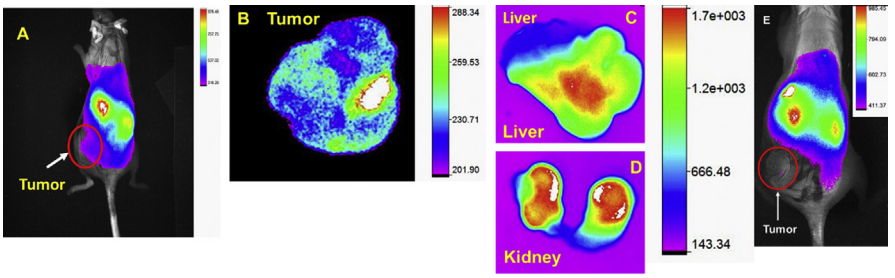

Fig. 8. HCC imaging of targeted formulation. (A) Whole body NIR fluorescence imaging of targeted PAMAM-Gal-S0456. Ex-vivo imaging of tumor (B), liver (C), kidney (D) after 14 h of post i.v injection, and (E) control-nanoparticle-dye treated mice. Higher tumor uptake was found in PAMAM-Gal-S0456 as compared to control dye treated mouse. The higher intensity of kidney as compared to liver indicates that PAMAM-Gal-S0456 is been excreted out through the kidneys.

4. Discussion

HCC is one of the most lethal and poor prognosis among all malignant aggressive liver cancer and it is still one of the major clinical challenges to physicians and patients even it is a small minority of cases in overall. As the HCCs are lacking early detection biomarkers, thus development of other biomarker specific theranostic drug delivery system is an urgent need for early detection and therapy [56, 59, 60]. ASGPRs receptors are highly overexpressed in HCC cells surface and can be a targeted site for drug delivery of nanocarriers containing targeting ligand to achieve active targeted delivery. Also, the poor aqueous solubility of currently investigated potent hydrophobic anticancer compounds like curcumin derivatives is a major obstacle in the way for their clinical translation potential. The CDF drug in this study has been shown to be a very promising anticancer flavonoid compound with the possibility to be efficient in several cancer cells but it has a major problem which is its poor aqueous solubility. This factor has made its systemic administration very problematic [60, 61]. Previously, our group has reported multiple studies which suggested that PAMAM dendrimers could enhance the solubility of various compounds and could satisfy the need to achieve anticancer drug accumulation at tumor site and minimize adverse side effects. Also, earlier we have been able to design variety of drug delivery systems for curcumin derivatives and other anticancer drugs such as our previously work indicated [30, 49, 55].

In this study, PAMAM dendrimer was selected because of their favorable characteristics for drug delivery [62] such as enhanced drug loading, better aqueous solubility and comparatively low toxicity profile (which can be further reduced by Galactosamine surface modification) [46]. Also, it is well reported that galactosamine is a selective targeting ligand for targeted anticancer drug delivery in HCCs due to its binding to the overexpressed (ASGPRs) with high affinity and the combo internalization into the cells through clathrin type receptor mediated endocytosis [40, 44]. Galactosamine was demonstrated to achieve ASGPR mediated efficient liver tumor targeting in phase

https://doi.org/10.1016/j.heliyon.2018.e01071

I clinical trial of poly[N-(2-hydroxypropyl)methacrylamide] copolymer carrying doxorubicin and galactosamine, as reported by Julyan and coworkers [45]. In the same line, Shen, et al. focused on the increased cellular uptake and cytotoxicity of galactosamine targeted doxorubicin loaded albumin nanoparticles compared to non-targeted particles [39, 50]. Similarly, Wang et al. showed that galactosamine conjugated micelles loaded with paclitaxel were of better drug internalization, cytotoxicity and induction of cell cycle arrest in contrast to the paclitaxel loaded micelles without galactosamine ligands [63]. As a result, galactosamine is a well-studied effective targeting tool for HCC cells expressing ASGPR. Galactosamine conjugated delivery systems could thus be very promising in achieving more effective HCC therapy, with better accumulation of therapeutic agents in the tumor tissue and lesser side effects.

In the present work, as a proof-of-concept we successfully conjugated GAL to G4 PAMAM dendrimers through succinic acid linkers. PAMAM-GAL systems combined the benefits of excellent drug delivery aspects inherited from PAMAM dendrimers and the unique and favorable binding of targeting ligand GAL to ASGPRs receptors on tumor cells. As a result, PAMAM-GAL was able to enhance the aqueous solubility of the anticancer compound (CDF) significantly. The higher CDF loading in CDF/PAMAM-GAL as compared to CDF/G4-PAMAM could be explained by the additional crowding of GAL ligands on the surface of PAMAM dendrimers. Conjugation with GAL provided steric hindrance that minimized CDF escaping from the hydrophobic cavities of PAMAM dendrimers. GAL conjugation also supported decreasing the surface positive charge of PAMAM dendrimer which is known to be responsible for PAMAM cytotoxicity. Our results are in concordance with previous reports, which also revealed better hydrophobic drug loading in ligand conjugated dendrimers [33].

In terms of particle size impact, it is generally known that size is one of the most important parameters in developing an ideal drug delivery system [56, 59, 64, 65, 66]. As illustrated in above results, it was concluded from hydrodynamic size and TEM assessments that both dendrimer formulations (CDF/G4-PAMAM and CDF/G4-PAMAM-GAL) were recognized to be in the ideal nano-metric range which suggested that the formulation can benefit from the enhanced permeability and retention (EPR) effect [67, 68, 69, 70, 71, 72] as well as from active targeting via galactosamine to selectively accumulate more in the tumor microenvironments than normal tissues area or non-targeted organs. Thus, the combination of higher accumulation in tumor site due to the EPR-effect and better cellular uptake by active targeting of GAL based formulation (CDF/PAMAM-GAL) to ASGPRs receptors on tumor cells is a key driving force to accumulate CDF in tumor site with increased therapeutic effect and minimized side-effects.

Regarding the particles surface charge, on the contrary of the Plain G4 PAMAM dendrimers which had positive zeta potential of around 13 mV $\pm$ 3.23 because of

https://doi.org/10.1016/j.heliyon.2018.e01071

their terminal protonated amine groups, the PAMAM-Gal dendrimers exposing galactosamine residues showed a low negative zeta potential of -8.3 ± 1.24 mV. This lowering in the zeta potential could be explained by the presence of anionic uncoupled succinic carboxylic groups on the PAMAM-Gal surface. Because of having negative zeta potential, PAMAM-GAL formulation had less potential to cause cytotoxicity effects when used for *in vivo* drug delivery testing which is crucial factor for developing effective and safe drug delivery vehicles.

Cytotoxicity evaluation demonstrated nontoxic behavior of PAMAM and PAMAM-GAL at the concentrations used indicating that they could be promising carriers for anticancer drug delivery. Our findings highlighted that CDF was more potent than Sorafenib, Doxorubicin, and Cisplatin which are all among the reported chemotherapeutic drugs used in treatment of advanced stages of hepatocellular carcinoma [16, 18, 19]. Thus, the more potent CDF could be more effective than all of them as a therapeutic agent for hepatic cancer. Importantly, the targeted formulation (CDF/PAMAM-GAL) showed highest anticancer activity at concentration range from 0.5 μM to 5 μM as compared to non-targeted formulation (CDF/G4-PAMAM) in Hep G2 cell lines. This could be explained by the targeting ability of GAL ligand that facilitates the PAMAM-GAL-CDF internalization into HepG2 cells overexpressing ASGPRs more efficiently than CDF/G4-PAMAM. This was confirmed by the amount of fluorescence intensity detected in the fluorescence microscopy study and the *in vivo* testing in the HCC mice model, which indicated the selective uptake of the targeted formulation via ASGPRs receptors mediated endocytosis. Overall, these results indicate that the targeted CDF/PAMAM-Gal formulation can show promising antitumor response and effective therapeutic role especially in HCC cancer with better accumulation of therapeutic agents in the tumor tissue and lesser side effects.

5. Conclusions

In this current study, PAMAM-GAL conjugate has been developed and showed great potential to be an excellent drug delivery system for CDF, a potent anticancer compound. The engineered nano-dendritic delivery system possesses numerous favorable properties such as enhancing the solubility of CDF with stable small nano-size (less than 50 nm), globular shape particles with a smooth surface morphology, and good drug loading content were obtained using dendrimer indicating its applicability for *in vivo* drug delivery. Also, biologically safety has been shown *in vitro* due to the shielding of positive charge of PAMAM dendrimer by GAL, potent *in vitro* anticancer activity and better internalization of targeted formulation with a high binding affinity to ASGPRs receptors compared to non-targeted formulations in HepG2 cells. Good *In vivo* bio-distribution results and selective accumulation in liver cancer has been demonstrated as well. Finally, the result

https://doi.org/10.1016/j.heliyon.2018.e01071

indicated that CDF/PAMAM-GAL could be a promising potential for systemic (targeted) anticancer therapy and imaging, warranting further *in vivo* investigations underway in our laboratory.

Declarations

Author contribution statement

Shaimaa Yousef, Samaresh Sau: Conceived and designed the experiments; Performed the experiments; Analyzed and interpreted the data; Wrote the paper.

Hashem O. Alsaab: Performed the experiments; Analyzed and interpreted the data; Wrote the paper.

Arun K. Iyer: Conceived and designed the experiments; Analyzed and interpreted the data; Contributed reagents, materials, analysis tools or data.

Funding statement

This work was supported by Wayne State University Start-up Funding.

Competing interest statement

The authors declare no conflict of interest.

Additional information

No additional information is available for this paper.

Acknowledgements

We acknowledge partial support for this work by Wayne State University Start-up funding to A.K.I. TEM analysis using JEOL 2010 was supported by an NSF Award #0216084.

References

[1] J. Ferlay, I. Soerjomataram, R. Dikshit, S. Eser, C. Mathers, M. Rebelo, D.M. Parkin, D. Forman, F. Bray, Cancer incidence and mortality worldwide: sources, methods and major patterns in GLOBOCAN 2012, Int. J. Cancer 136 (2015) E359−E386.

[2] A.B. Ryerson, C.R. Eheman, S.F. Altekruse, J.W. Ward, A. Jemal, R.L. Sherman, S.J. Henley, D. Holtzman, A. Lake, A.-M. Noone, R.N. Anderson, J. Ma, K.N. Ly, K.A. Cronin, L. Penberthy, B.A. Kohler,

https://doi.org/10.1016/j.heliyon.2018.e01071

Annual report to the nation on the status of cancer, 1975−2012, featuring the increasing incidence of liver cancer, Cancer 122 (2016) 1312−1337.

[3] R.L. Siegel, K.D. Miller, A. Jemal, Cancer statistics, 2016, CA Cancer J. Clin. 66 (2016) 7−30.

[4] R.L. Siegel, K.D. Miller, A. Jemal, Cancer statistics, 2018, CA Cancer J. Clin. 68 (2018) 7−30.

[5] M.C.S. Wong, J.Y. Jiang, M. Liang, Y. Fang, M.S. Yeung, J.J.Y. Sung, Global temporal patterns of pancreatic cancer and association with socioeconomic development, Sci. Rep. 7 (2017) 3165.

[6] H.B. El-Serag, Hepatocellular carcinoma: an epidemiologic view, J. Clin. Gastroenterol. 35 (2002) S72−S78.

[7] J.-W. Lu, Y.-J. Ho, Y.-J. Yang, H.-A. Liao, S.-C. Ciou, L.-I. Lin, D.-L. Ou, Zebrafish as a disease model for studying human hepatocellular carcinoma, World J. Gastroenterol. 21 (2015) 12042−12058.

[8] M.C. Kew, H. Popper, Relationship between hepatocellular carcinoma and cirrhosis, Semin. Liver Dis. 4 (1984) 136−146.

[9] H. Poustchi, S. Sepanlou, S. Esmaili, N. Mehrabi, A. Ansarymoghadam, Hepatocellular carcinoma in the world and the middle East, Middle East J. Dig. Dis. 2 (2010) 31−41.

[10] M. Schwartz, S. Roayaie, M. Konstadoulakis, Strategies for the management of hepatocellular carcinoma, Nat. Clin. Pract. Oncol. 4 (2007) 424−432.

[11] D. Janevska, V. Chaloska-Ivanova, V. Janevski, Hepatocellular carcinoma: risk factors, diagnosis and treatment, open access maced, J. Med. Sci. 3 (2015) 732−736.

[12] T. Livraghi, Radiofrequency ablation, PEIT, and TACE for hepatocellular carcinoma, J. Hepatobiliary Pancreat. Surg. 10 (2003) 67−76.

[13] J.M. Llovet, M.I. Real, X. Montaña, R. Planas, S. Coll, J. Aponte, C. Ayuso, M. Sala, J. Muchart, R. Solà, J. Rodés, J. Bruix, Barcelona Liver Cancer Group, Arterial embolisation or chemoembolisation versus symptomatic treatment in patients with unresectable hepatocellular carcinoma: a randomised controlled trial, Lancet (London, England) 359 (2002) 1734−1739.

[14] S. Shiina, T. Teratani, S. Obi, S. Sato, R. Tateishi, T. Fujishima, T. Ishikawa, Y. Koike, H. Yoshida, T. Kawabe, M. Omata, A randomized controlled trial of

https://doi.org/10.1016/j.heliyon.2018.e01071

radiofrequency ablation with ethanol injection for small hepatocellular carcinoma, Gastroenterology 129 (2005) 122–130.

[15] V. Mazzaferro, E. Regalia, R. Doci, S. Andreola, A. Pulvirenti, F. Bozzetti, F. Montalto, M. Ammatuna, A. Morabito, L. Gennari, Liver transplantation for the treatment of small hepatocellular carcinomas in patients with cirrhosis, N. Engl. J. Med. 334 (1996) 693–699.

[16] A.X. Zhu, Systemic therapy of advanced hepatocellular carcinoma: how hopeful should we be? Oncologist 11 (2006) 790–800.

[17] F. Capone, E. Guerriero, A. Sorice, G. Colonna, G. Storti, J. Pagliuca, G. Castello, S. Costantini, Synergistic antitumor effect of Doxorubicin and tacrolimus (FK506) on hepatocellular carcinoma cell lines, ScientificWorldJournal 2014 (2014) 450390.

[18] S.H. Wrzesinski, T.H. Taddei, M. Strazzabosco, Systemic therapy in hepatocellular carcinoma, Clin. Liver Dis. 15 (2011) 423–441, vii–x.

[19] G.-L. Deng, S. Zeng, H. Shen, Chemotherapy and target therapy for hepatocellular carcinoma: new advances and challenges, World J. Hepatol. 7 (2015) 787–798.

[20] M. Kudo, Immuno-oncology in hepatocellular carcinoma: 2017 update, Oncology (2017).

[21] H.O. Alsaab, S. Sau, R. Alzhrani, K. Tatiparti, K. Bhise, S.K. Kashaw, A.K. Iyer, PD-1 and PD-L1 checkpoint signaling inhibition for cancer immunotherapy: mechanism, combinations, and clinical outcome, Front. Pharmacol. 8 (2017) 1–15.

[22] S. Sau, H.O. Alsaab, K. Bhise, R. Alzhrani, G. Nabil, A.K. Iyer, Multifunctional nanoparticles for cancer immunotherapy: a groundbreaking approach for reprogramming malfunctioned tumor environment, J. Control. Release 274 (2018) 24–34.

[23] H.O. Alsaab, S. Sau, R.M. Alzhrani, V.T. Cheriyan, L.A. Polin, U. Vaishampayan, A.K. Rishi, A.K. Iyer, Tumor hypoxia directed multimodal nanotherapy for overcoming drug resistance in renal cell carcinoma and reprogramming macrophages, Biomaterials 183 (2018) 280–294.

[24] A. Kato, M. Miyazaki, S. Ambiru, H. Yoshitomi, H. Ito, K. Nakagawa, H. Shimizu, O. Yokosuka, N. Nakajima, Multidrug resistance gene (MDR-1) expression as a useful prognostic factor in patients with human hepatocellular carcinoma after surgical resection, J. Surg. Oncol. 78 (2001) 110–115.

https://doi.org/10.1016/j.heliyon.2018.e01071

[25] M. Huang, G. Liu, The study of innate drug resistance of human hepatocellular carcinoma Bel7402 cell line, Cancer Lett. 135 (1999) 97−105.

[26] D. Kim, M.-D. Kim, C.-W. Choi, C.-W. Chung, S. Ha, C. Kim, Y.-H. Shim, Y.-I. Jeong, D. Kang, E. Allemann, R. Gurny, E. Doelker, R. Gref, Y. Minamitake, M. Peracchia, V. Trubetskoy, V. Torchilin, R. Langer, S. La, T. Okano, K. Kataoka, G. Kwon, M. Naito, M. Yokoyama, T. Okano, Y. Sakurai, K. Kataoka, G. Kwon, M. Naito, M. Yokoyama, G. Kwon, M. Yokoyama, T. Okano, Y. Sakurai, K. Kataoka, D. Seehofer, C. Kamphues, P. Neuhaus, S. Wilhelm, L. Adnane, P. Newell, A. Villanueva, J. Llovet, M. Lynch, L. Liu, Y. Cao, C. Chen, X. Zhang, A. McNabola, D. Wilkie, S. Wilhelm, M. Lynch, C. Carter, W. Qun, Y. Tao, X. Wang, J. Fan, Y. Liu, B. Zhao, Z. Jia, Q. Zhang, J. Zhang, B. He, W. Qu, Z. Cui, Y. Wang, H. Zhang, J. Wang, Q. Zhang, Y. Jeong, D. Kim, C. Chung, J. Yoo, K. Choi, C. Kim, S. Ha, D. Kang, Y. Jeong, D. Kim, M. Jang, J. Nah, Y. Kim, Antitumor activity of sorafenib-incorporated nanoparticles of dextran/poly(dl-lactide-co-glycolide) block copolymer, Nanoscale Res. Lett. 7 (2012) 91.

[27] P. Kesharwani, S. Banerjee, S. Padhye, F.H. Sarkar, A.K. Iyer, Parenterally administrable nano-micelles of 3,4-difluorobenzylidene curcumin for treating pancreatic cancer, Colloids Surf. B Biointerfaces 132 (2015) 138−145.

[28] Z. Wang, S. Sau, H.O. Alsaab, A.K. Iyer, CD44 directed nanomicellar payload delivery platform for selective anticancer effect and tumor specific imaging of triple negative breast cancer, Nanomed. Nanotechnol. Biol. Med. 14 (4) (June 2018) 1441−1454.

[29] B. Bao, S. Ali, S. Banerjee, Z. Wang, F. Logna, A.S. Azmi, D. Kong, A. Ahmad, Y. Li, S. Padhye, F.H. Sarkar, Curcumin analogue CDF inhibits pancreatic tumor growth by switching on suppressor microRNAs and attenuating EZH2 expression, Cancer Res. 72 (2012) 335−345.

[30] D. Luong, S. Sau, P. Kesharwani, A.K. Iyer, Polyvalent folate-dendrimer-coated iron oxide theranostic nanoparticles for simultaneous magnetic resonance imaging and precise cancer cell targeting, Biomacromolecules 18 (4) (2017) 1197−1209.

[31] N. Duhem, F. Danhier, V. Pourcelle, J.M. Schumers, O. Bertrand, C.S. Leduff, S. Hoeppener, U.S. Schubert, J.F. Gohy, J. Marchand-Brynaert, V. Prat, Self-assembling doxorubicin-tocopherol succinate prodrug as a new drug delivery system: synthesis, characterization, and in vitro and in vivo anticancer activity, Bioconjug. Chem. 25 (2014) 72−81.

https://doi.org/10.1016/j.heliyon.2018.e01071

[32] D. Luong, P. Kesharwani, H.O. Alsaab, S. Sau, S. Padhye, F.H. Sarkar, A.K. Iyer, Folic acid conjugated polymeric micelles loaded with a curcumin difluorinated analog for targeting cervical and ovarian cancers, Colloids Surf. B Biointerfaces 157 (2017) 490−502.

[33] D. Luong, P. Kesharwani, B.A. Killinger, A. Moszczynska, F.H. Sarkar, S. Padhye, A.K. Rishi, A.K. Iyer, Solubility enhancement and targeted delivery of a potent anticancer flavonoid analogue to cancer cells using ligand decorated dendrimer nano-architectures, J. Colloid Interface Sci. 484 (2016) 33−43.

[34] P.R. Dandawate, A. Vyas, A. Ahmad, S. Banerjee, J. Deshpande, K.V. Swamy, A. Jamadar, A.C. Dumhe-Klaire, S. Padhye, F.H. Sarkar, Inclusion complex of novel curcumin analogue CDF and β-cyclodextrin (1:2) and its enhanced in vivo anticancer activity against pancreatic cancer, Pharm. Res. 29 (2012) 1775−1786.

[35] A. Ahmad, A. Sayed, K.R. Ginnebaugh, V. Sharma, A. Suri, A. Saraph, S. Padhye, F.H. Sarkar, Molecular docking and inhibition of matrix metalloproteinase-2 by novel difluorinatedbenzylidene curcumin analog, Am. J. Transl. Res. 7 (2015) 298.

[36] S. Ali, A. Ahmad, S. Banerjee, S. Padhye, K. Dominiak, J.M. Schaffert, Z. Wang, P.A. Philip, F.H. Sarkar, Gemcitabine sensitivity can be induced in pancreatic cancer cells through modulation of miR-200 and miR-21 expression by curcumin or its analogue CDF, Cancer Res. (2010) 8−5472.

[37] B. Bao, S. Ali, D. Kong, S.H. Sarkar, Z. Wang, S. Banerjee, A. Aboukameel, S. Padhye, P.A. Philip, F.H. Sarkar, Anti-tumor activity of a novel compound-CDF is mediated by regulating miR-21, miR-200, and pten in pancreatic cancer, PLoS One 6 (2011) 1−12.

[38] M. Ahmed, R. Narain, Carbohydrate-based materials for targeted delivery of drugs and genes to the liver, Nanomedicine (2015).

[39] Z. Shen, W. Wei, H. Tanaka, K. Kohama, G. Ma, T. Dobashi, Y. Maki, H. Wang, J. Bi, S. Dai, A galactosamine-mediated drug delivery carrier for targeted liver cancer therapy, Pharmacol. Res. 64 (2011) 410−419.

[40] P.O. Pathak, M.S. Nagarsenker, C.R. Barhate, S.G. Padhye, V.V. Dhawan, D. Bhattacharyya, C.L. Viswanathan, F. Steiniger, A. Fahr, Cholesterol anchored arabinogalactan for asialoglycoprotein receptor targeting: synthesis, characterization, and proof of concept of hepatospecific delivery, Carbohydr. Res. 408 (2015) 33−43.

https://doi.org/10.1016/j.heliyon.2018.e01071

[41] D. Trerè, L. Fiume, L.B. De Giorgi, G. Di Stefano, M. Migaldi, M. Derenzini, The asialoglycoprotein receptor in human hepatocellular carcinomas: its expression on proliferating cells, Br. J. Cancer 81 (1999) 404−408.

[42] M. Singh, M. Ariatti, Targeted gene delivery into HepG2 cells using complexes containing DNA, cationized asialoorosomucoid and activated cationic liposomes, J. Control. Release 92 (2003) 383−394.

[43] D.-J. Peng, J. Sun, Y.-Z. Wang, J. Tian, Y.-H. Zhang, M.H.M. Noteborn, S. Qu, Inhibition of hepatocarcinoma by systemic delivery of Apoptin gene via the hepatic asialoglycoprotein receptor, Cancer Gene Ther. 14 (2007) 66−73.

[44] R.T. Lee, P. Lin, Y.C. Lee, New synthetic cluster ligands for galactose/N-acetylgalactosamine-specific lectin of mammalian liver, Biochemistry 23 (1984) 4255−4261.

[45] P.J. Julyan, L.W. Seymour, D.R. Ferry, S. Daryani, C.M. Boivin, J. Doran, M. David, D. Anderson, C. Christodoulou, A.M. Young, S. Hesslewood, D.J. Kerr, Preliminary clinical study of the distribution of HPMA copolymers bearing doxorubicin and galactosamine, J. Control. Release 57 (1999) 281−290.

[46] K. Bhise, S. Sau, H. Alsaab, S.K. Kashaw, R.K. Tekade, A.K. Iyer, Nanomedicine for cancer diagnosis and therapy: advancement, success and structure–activity relationship, Ther. Deliv. 8 (2017) 1003−1018.

[47] S. Sau, H.O. Alsaab, S.K. Kashaw, K. Tatiparti, A.K. Iyer, Advances in antibody-drug conjugates: a new era of targeted cancer therapy, Drug Discov. Today 22 (10) (2017 Oct) 1547−1556.

[48] S. Ueno, M. Mojic, Y. Ohashi, N. Higashi, Y. Hayakawa, T. Irimura, Asialoglycoprotein receptor promotes cancer metastasis by activating the EGFR-ERK pathway, Cancer Res. (2011).

[49] H. Alsaab, R. Alzhrani, P. Kesharwani, S. Sau, S. Boddu, A. Iyer, Folate decorated nanomicelles loaded with a potent curcumin analogue for targeting retinoblastoma, Pharmaceutics 9 (2017) 15.

[50] C. Yan, D. Chen, J. Gu, H. Hu, X. Zhao, M. Qiao, Preparation of N-succinyl-chitosan and its physical-chemical properties as a novel excipient, Yakugaku Zasshi 126 (2006) 789−793.

[51] J. Wang, B. Dou, Y. Bao, Efficient targeted pDNA/siRNA delivery with folate-low-molecular-weight polyethyleneimine-modified pullulan as non-viral carrier, Mater. Sci. Eng. C 34 (2014) 98−109.

https://doi.org/10.1016/j.heliyon.2018.e01071

[52] K. Tatiparti, S. Sau, K. Gawde, A. Iyer, Copper-free 'Click' chemistry-based synthesis and characterization of carbonic anhydrase-IX anchored albumin-paclitaxel nanoparticles for targeting tumor hypoxia, Int. J. Mol. Sci. 19 (2018) 838.

[53] K. Bhise, S.K. Kashaw, S. Sau, A.K. Iyer, Nanostructured lipid carriers employing polyphenols as promising anticancer agents: quality by design (QbD) approach, Int. J. Pharm. 526 (1–2) (2017 Jun 30) 506–515.

[54] P. Sahu, S.K. Kashaw, S. Jain, S. Sau, A.K. Iyer, Assessment of penetration potential of pH responsive double walled biodegradable nanogels coated with eucalyptus oil for the controlled delivery of 5-fluorouracil: in vitro and ex vivo studies, J. Control. Release 253 (2017) 122–136.

[55] K.A. Gawde, P. Kesharwani, S. Sau, F.H. Sarkar, S. Padhye, S.K. Kashaw, A.K. Iyer, Synthesis and characterization of folate decorated albumin bioconjugate nanoparticles loaded with a synthetic curcumin difluorinated analogue, J. Colloid Interface Sci. 496 (2017) 290–299.

[56] A.I. Almansour, N. Arumugam, R. Suresh Kumar, S.M. Mahalingam, S. Sau, G. Bianchini, J.C. Menéndez, M. Altaf, H.A. Ghabbour, Design, synthesis and antiproliferative activity of decarbonyl luotonin analogues, Eur. J. Med. Chem. 138 (2017) 932–941.

[57] C.F. Shum, C.D. Bahler, P.S. Low, T.L. Ratliff, S.V. Kheyfets, J.P. Natarajan, G.E. Sandusky, C.P. Sundaram, Novel use of folate-targeted intraoperative fluorescence, OTL38, in robot-assisted laparoscopic partial nephrectomy: report of the first three cases, J. Endourol. Case Rep. 2 (2016) 189–197.

[58] P.C. Lv, J. Roy, K.S. Putt, P.S. Low, Evaluation of a carbonic anhydrase IX-targeted near-infrared dye for fluorescence-guided surgery of hypoxic tumors, Mol. Pharm. 13 (2016) 1618–1625.

[59] R. Anjibabu, S. Sau, B.J.M. Reddy, R. Banerjee, B.V.S. Reddy, Heteropoly acid catalyzed synthesis of 8-methyl-2-aryl/alkyl-3- oxabicyclo[3.3.1]non-7-ene derivatives through (3,5)-oxonium-ene reaction, Tetrahedron Lett. 54 (2013) 7160–7163.

[60] V.T. Cheriyan, H.O. Alsaab, S. Sekhar, C. Stieber, A.K. Iyer, A.K. Rishi, A CARP-1 functional mimetic loaded vitamin E-TPGS micellar nanoformulation for inhibition of renal cell carcinoma, Oncotarget 8 (62) (2017 Dec 1) 104928–104945.

[61] J.M. Wickens, H.O. Alsaab, P. Kesharwani, K. Bhise, M.C.I.M. Amin, R.K. Tekade, U. Gupta, A.K. Iyer, Recent advances in hyaluronic acid-decorated nanocarriers for targeted cancer therapy, Drug Discov. Today 22 (2016) 665–680.

https://doi.org/10.1016/j.heliyon.2018.e01071

[62] A.K. Sharma, A. Gothwal, P. Kesharwani, H. Alsaab, A.K. Iyer, U. Gupta, Dendrimer nanoarchitectures for cancer diagnosis and anticancer drug delivery, Drug Discov. Today 22 (2) (2017) 314–326.

[63] Y.-C. Wang, X.-Q. Liu, T.-M. Sun, M.-H. Xiong, J. Wang, Functionalized micelles from block copolymer of polyphosphoester and poly(epsilon-caprolactone) for receptor-mediated drug delivery, J. Control. Release 128 (2008) 32–40.

[64] S. Sau, R. Banerjee, Cationic lipid-conjugated dexamethasone as a selective antitumor agent, Eur. J. Med. Chem. 83 (2014) 433–447.

[65] S. Mukherjee, S. Sau, D. Madhuri, V.S. Bollu, K. Madhusudana, B. Sreedhar, R. Banerjee, C.R. Patra, Green synthesis and characterization of monodispersed gold nanoparticles: toxicity study, delivery of doxorubicin and its bio-distribution in mouse model, J. Biomed. Nanotechnol. 12 (2016) 165–181.

[66] S. Sau, P. Agarwalla, S. Mukherjee, I. Bag, B. Sreedhar, M. Pal-Bhadra, C.R. Patra, R. Banerjee, Cancer cell-selective promoter recognition accompanies antitumor effect by glucocorticoid receptor-targeted gold nanoparticle, Nanoscale 6 (2014) 6745–6754.

[67] J. Fang, H. Nakamura, H. Maeda, The EPR effect: unique features of tumor blood vessels for drug delivery, factors involved, and limitations and augmentation of the effect, Adv. Drug Deliv. Rev. 63 (2011) 136–151.

[68] K. Greish, Enhanced permeability and retention effect for selective targeting of anticancer nanomedicine: are we there yet? Drug Discov. Today Technol. 9 (2012) e161–e166.

[69] V. Torchilin, Tumor delivery of macromolecular drugs based on the EPR effect, Adv. Drug Deliv. Rev. 63 (2011) 131–135.

[70] H. Maeda, Toward a full understanding of the EPR effect in primary and metastatic tumors as well as issues related to its heterogeneity, Adv. Drug Deliv. Rev. 91 (2015) 3–6.

[71] H. Maeda, H. Nakamura, J. Fang, The EPR effect for macromolecular drug delivery to solid tumors: improvement of tumor uptake, lowering of systemic toxicity, and distinct tumor imaging in vivo, Adv. Drug Deliv. Rev. 65 (2013) 71–79.

[72] A.K. Iyer, G. Khaled, J. Fang, H. Maeda, Exploiting the enhanced permeability and retention effect for tumor targeting, Drug Discov. Today 11 (2006) 812–818.

https://doi.org/10.1016/j.heliyon.2018.e01071